Classical-trajectory calculations on Ar^+ sputtering of a Si(001) surface using an *ab initio* potential

Robert A. Stansfield, Keith Broomfield, and David C. Clary
University Chemical Laboratory, University of Cambridge, Lensfield Road, Cambridge CB2 1EW, England
(Received 27 December 1988)

We describe classical-trajectory calculations of sputtering yields for Ar^+-ion collisions with a Si(001) surface. The Ar^+-Si and short-ranged Si-Si interaction potentials were calculated using the *ab initio* Hartree-Fock and configuration-interaction methods. The low-energy potential describing the silicon solid is the two- and three-body form due to Stillinger and Weber. We compare the calculated sputtering yields with experiment. The potential-energy surface strongly influences the calculated sputtering yields, and it is found that the most reasonable agreement is obtained from our potentials using the (2×1) Si(001) reconstructed surface rather than the bulk-terminated surface. Analysis of the kinetic energy and angular distributions of the sputtered silicon atoms and of cluster yields has provided a mechanism of ejection.

I. INTRODUCTION

The development of the electronics industry during the last 25 years has seen a rapid growth in the complexity of integrated circuits (IC's) from the small-scale integration of the early 1960s to the very-large-scale integration (VLSI) circuits of today. The most common material for these circuits is silicon, though there is increasing interest in the use of compound semiconductors such as gallium arsenide. The fundamental problem in the manufacturing process is that as the dimensions of the VLSI chip are reduced, and the number of components per chip is increased, the degree of control over the manufacturing processes must be necessarily improved.[1]

In VLSI microfabrication, it is particularly desirable to choose an anisotropic process, i.e, a process for which the vertical etch rate is much greater than the lateral etch rate, so that undercutting of the mask is minimized and the features making up the circuits can be packed much closer together. One way of achieving this is by dry etching, either by direct ion bombardment[2–6] or by ion-beam-assisted etching (IBAE) (Refs. 7–12) and plasma etching.[13–23] IBAE and plasma etching are particularly anisotropic because, since the ion flux is normal to the substrate surface, the bottom of the feature being cut in the substrate receives a much greater flux of energetic ions than the sidewalls.[24] The chemistry of IBAE has recently been reviewed by Mayer, Ameen, and Vitkavage.[25]

Another important process is that of ion implantation,[26] where silicon wafers are n-type and p-type doped by 3–500-keV ion beams of boron, phosphorus, and arsenic. Using this technique, precise control may be obtained over the depth profile and concentration of the dopants. However, there is a limit on the maximum concentration profile that may be achieved since the already implanted atoms may be resputtered.

However, in spite of the technological importance of these processes, there has been little theoretical investigation of the factors governing the sputtering of silicon. In this paper, we present results of classical-trajectory calculations of argon-ion sputtering of silicon. While the sputtering of metals has been intensively investigated by classical-trajectory simulations,[27–32] almost no attention has been paid to the sputtering of silicon and other semiconductors. The reason for this is readily apparent: two-body potentials stabilize closed-packed structures and thus descriptions of the potential-energy surface of an open crystal form such as the diamond cubic lattice of silicon and germanium requires the use of computationally expensive many-body potential functions. These factors make this system a benchmark for the use of many-body potentials in a computer simulation.

Classical-trajectory calculations require the knowledge of interatomic potentials, and in the literature there are many potentials available for silicon, though not all of them are suitable for sputtering simulations. The simplest of the various proposed silicon potentials is that due to Halicioğlu *et al.*,[33–35] in which the two-body term is a Lennard-Jones function[36] and the three-body part is derived from an Axilrod-Teller potential.[37] A more accurate description of the properties of silicon was obtained using the Keating-model potential,[38] where interactions are expressed in terms of bond stretches and bends, and interactions between the stretches and bends. Unfortunately, this potential is not suitable for describing disordered systems. Biswas and Hamman[39,40] have devised potentials to describe the cohesive energies of silicon clusters, and Tersoff[41,42] has derived two-body potentials which are dependent on the local environment.

The bulk silicon potential function which has gained widest acceptance in recent years is that due to Stillinger and Weber.[43] Unlike other proposed potentials[34,39–45] which were fitted to ordered systems such as the perfect diamond lattice, this potential was optimized to describe the dynamics of both the solid and liquid phases. For this reason, the Stillinger-Weber potential is considered to be the best available for situations which may involve a large amount of disorder or number of defects.[46] The po-

tential has been successfully applied to a variety of problems ranging from the dynamics of liquid[47] and amorphous[48] silicon, the properties of the crystal-melt interface,[49–52] and the fragmentation of silicon microclusters.[53] However phonon dispersion curves calculated using this potential are in poor agreement with experiment,[45] and the elastic constants of the perfect diamond lattice are found to be 30–40% too high.[54] The functional form of this potential is especially suitable for classical-trajectory simulations since the potential goes smoothly to zero at a cutoff distance between the first- and second-nearest-neighbor distances of the equilibrium lattice structure, thus minimizing the number of interactions that must be calculated at each time step.

Recently, Brenner and Garrison[45] developed an alternative potential for silicon based on a modification of Keating's valence-force field.[38] Unlike the Stillinger-Weber potential, this potential is able to accurately reproduce the phonon dispersion relations of the silicon lattice, indicating that the true potential-energy surface is being described very accurately at near equilibrium geometry. Molecular-dynamics simulations of the solid state give favorable results when compared with experiment,[45] but the potential has not yet been used to study the dynamics of the liquid and amorphous states which would provide a better test of its suitability for sputtering calculations. Simulations using this potential involve an increased expense in computer time compared to the Stillinger-Weber potential because, although the Brenner-Garrison potential also goes smoothly to zero between the first- and second-nearest-neighbor distances, the additional complexity of the functional form means that the third-body forces are very costly to evaluate.

We now consider the initial conditions of the trajectory calculations. Sputtering calculations in the past have generally neglected the small relaxations of surface atoms away from the bulk equilibrium geometry, since they were found to have a negligible influence on the dynamics.[55,56] However, for Si(001), the surface reconstruction involves major displacements of selvage atoms from the bulk geometry, and this might be expected to have an appreciable effect on the calculated trajectories. Unfortunately, the exact nature of the reconstruction of the Si(001) surface remains in some doubt. It is now accepted that the dimer pairing model of Schlier and Farnsworth[57] as deduced on the basis of the low-energy electron diffraction (LEED) experiments is the correct basic description of the reconstruction. In this model, one of the two dangling bonds per surface atom forms a new bond with a corresponding dangling bond of a neighboring atom. The consequence of this is that the two atoms are displaced from their bulk geometries towards each other, forming a (2×1) reconstructed surface. However, higher-order LEED spots, such as the $c(4\times2)$ pattern observed by Lander and Morrison,[58] have long indicated that this cannot be the complete description.

Chadi[59] and Yin and Cohen[60] have performed tight-binding total-energy calculations to determine the minimum-energy structure of the reconstructed Si(001) surface. These calculations predict that the surface dimers were both asymmetric (i.e., one atom within the dimer was displaced further from its bulk position than the other) and buckled (i.e., one atom is raised upwards relative to the other). Variously proposed models of this surface reconstruction have been reviewed recently by Schlüter.[61]

Since classical-trajectory simulations of sputtering describe the dynamics of the surface layers of the target, it is essential that the potential-energy function chosen to model the interactions between the solid atoms be able to reproduce surface properties such as the equilibrium surface geometry. This need not be the case since solid potential functions are generally fitted to bulk properties where the electron-density distribution may be very different.[62] Abraham and Batra[63] have used the Stillinger-Weber potential to determine the equilibrium geometry of the (2×1) Si(001) reconstructed surface and found that buckled and twisted dimers were unstable with respect to the symmetric dimer. However, since buckling and twisting involves charge transfer between the dimer atoms,[59] which the Stillinger-Weber potential is unable to describe, this result is not too unexpected. Self-consistent tight-binding calculations by Bechstedt and Reichardt[64] indicate that the energy gain in forming buckled and twisted dimers from the perfect (2×1) reconstructed surface is only of the order of 0.04 eV and that the amount of twisting and buckling is small. This is in good agreement with scanning tunneling microscopy studies by Tromp *et al.*,[65,66] who find that the numbers of buckled and nonbuckled dimers are roughly equal. More recent molecular-dynamics calculations predict that the Si(001) surface is composed of islands of (2×1) dimer reconstruction separated by regions of disorder,[46] which is in good agreement with the results of Tromp *et al.* The Stillinger-Weber potential has been used to study the solid-liquid-melt interface,[49] epitaxial growth from the liquid phase[51,52] and by use of molecular beams,[67,68] pulsed laser melting of the surface,[69] and in calculations of the adatom vibrations on the reconstructed surface.[70] The Brenner-Garrison potential has been less extensively tested but has been used with similar success in surface simulations.[71–73]

The earliest application of classical-trajectory methods to the sputtering of a semiconductor were by Ostry *et al.*[74,75] and Smith[76] on the Ar^+ bombardment of germanium and silicon, respectively. These studies used the metastable model of Harrison, Jr. *et al.*,[77] in which the pair-potential functions are eroded at the equilibrium interatomic separation and the binding forces are modeled by a planar barrier. This removed the need for many-body potential functions to maintain the lattice structure. Ostry *et al.* used an Abrahamson[78] Born-Mayer potential at high energy matched to a Morse potential at low energy to describe the Ge-Ge interaction while Smith calculated a new silicon potential using the modified Wedepohl method.[79–81] These calculations examined various sputtering mechanisms within the diamond cubic lattice and comparisons of the angular distributions of the sputtered atoms and the relative sputtering yields between the different crystal faces with experiment were generally favorable.

Calculations using the full classical-trajectory method

have been relatively few. Park and Clary[82] have performed calculations on the sputtering of silicon by Ar^+ ions in the presence of a chlorine overlayer, but they neglected the third-body terms in the potential surface, relying on clamped atoms at the edge of the lattice to maintain the stability of the lattice for the duration of each trajectory. More recently, Lampinen *et al.*[68] and Brenner and Garrison[71,73] have studied the molecular-beam epitaxy of silicon using many-body potentials. However, no studies of the sputtering of silicon using a many-body potential have previously been performed.

The great difficulty encountered when comparing experimental sputtering yields with those determined by computer simulation is that the latter are an average of many ion collisions with an undamaged surface, while the former are the average of many ion collisions with the same surface. Blank and Wittmaack[83] and Kempf[84] have investigated the variation of the sputtering yields of silicon bombarded by argon and xenon ions with dosage and found that the sputtering yield increased with increasing dosage until steady-state conditions were achieved. This was found to correlate with the amount of implanted rare-gas atoms in the surface region, and the consequential reduction in the surface binding energy. In addition, semiconductors are readily amorphized under ion bombardment, so that the influence of the lattice structure on the sputtering yield may be easily lost.[85–87] Consequently, direct comparison between experiment and theory is only possible provided the experiments are performed in "low-dose" mode under which circumstances the amount of damage to and implantation in the surface will be minimal.

Recently, Winograd *et al.*[88] have developed a new method which enables the determination of low-dose sputtering yields, and energy and angle-resolved distributions of neutral atoms (EARN) desorbed from surfaces. However, the only experimental data presently available are for argon-ion sputtering of rhodium surfaces,[27,88] and for other systems it remains necessary to rely on unsuitable experimental sputtering yields for the purpose of comparison of theory with experiment.

In a previous paper,[89] we showed that a satisfactory agreement between calculated and experimental sputtering yields for Ar^+-Cu(100) is obtained when using pair potentials calculated using *ab initio* electronic-structure theory, rather than analytic potentials. It was found that the inclusion of electron correlation effects is necessary to obtain an accuracy of ± 0.1 eV. A similar method is adopted in this paper for the calculation of Ar^+-Si and Si-Si potentials.

In the following section, the new Si-Si and Ar^+-Si potentials are described and compared to previously proposed potentials. In Sec. III, the classical-trajectory simulations of the sputtering of the Si(001) surface by Ar^+ ions will be described. Section IV contains the results and discussion. Conclusions are presented in Sec. V.

II. THE Si-Si and Ar^+-Si REPULSIVE POTENTIALS

The Stillinger-Weber and Brenner-Garrison potentials were both developed for the purpose of modeling the

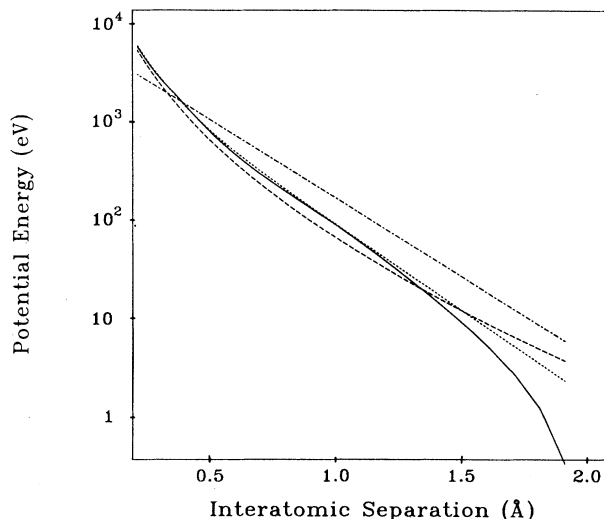

FIG. 1. A comparison of the SCF and empirical Ar^+-Si potentials. (——) denotes the SCF potential, (· · · ·) denotes the Smith modified Wedepohl potential, (— — —) denotes the Biersack-Ziegler universal potential, and (—·—·—·) denotes the Abrahamson potential.

low-energy dynamical properties of silicon. Neither provides an acceptable description of the potential-energy surface at energies above a few eV. At short interatomic separations, the Stillinger-Weber two-body term varies as r^{-4} while Brenner and Garrison originally employed a Gaussian function. Recently, Brenner replaced the Gaussian term with a high-energy potential function[72] which appears to be that of Smith.[76]

Since none of these, nor the previously used Morse and Abrahamson potentials, are expected to provide an accu-

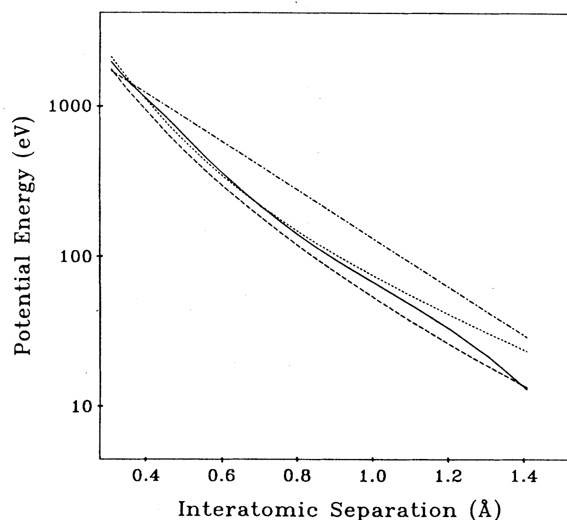

FIG. 2. A comparison of the SDCI and empirical Si-Si potentials. (——) denotes the SDCI potential, (· · · ·) denotes the Smith modified Wedepohl potential, (— — —) denotes the Biersack-Ziegler universal potential, and (—·—·—·) denotes the Abrahamson potential.

rate description of the potential-energy surface at high energies, we have calculated new potentials using electronic-structure theory in a similar way to our previous study of argon-ion sputtering of copper.[89] Each silicon atom within the perfect solid forms a single bond to each of its four neighboring atoms. Since the ground state of the Si_2 dimer is the inappropriate double-bonded $^3\Sigma_g^-$ state, the tetrahedrally disposed single bonds of the bulk silicon were imposed by performing the calculations on the Si_2H_6 molecule. The hydrogens were kept fixed at the exact tetrahedral geometry over the range of Si-Si interatomic separations considered, and a staggered conformation was maintained throughout. The Si—H bond length was kept constant throughout the calculations at the experimental value for SiH_4 (Ref. 90) (1.4798 Å) as used by Rothenberg *et al.*[91] Similarly, the SiH_3Ar^+ molecule was used for the Ar^+-Si potential. For the Ar and Si basis sets we used triple-ζ contractions of those of Veillard[92] with two *d* polarization functions added from the set in Huzinaga's compilation,[93] i.e., $(12s9p2d/9s6p2d)$, while for H the basis set of Dunning[94,95] was used with one *p*-polarization function added of exponent of 1.0, i.e., $(4s1p/2s1p)$. The basis sets are shown in Table I.

For the Si-Si potential, our calculations show that correlation has an appreciable effect on the shape of the calculated potential. At short interatomic separations there is about 0.5 eV less correlation energy than at bonding distances, and the variation in correlation energy was not smooth, the maximum being 0.8 eV, so this potential was calculated using the singles and doubles configuration-interaction (SDCI) method involving all electrons in the full molecular-orbital basis set. Although the molecule had full D_{3d} symmetry, the CI calculations were carried out in C_{2h} symmetry for technical reasons.

TABLE I. Unnormalized contracted Gaussian-type orbital (GTO) basis sets.

	Si			Ar			H	
	Exponents	Coefficients		Exponents	Coefficients		Exponents	Coefficients
s	699 89.3	0.000 31	*s*	118 186.0	0.000 30	*s*	19.2406	0.032 828
	103 80.2	0.002 49		17 688.8	0.002 38		2.8992	0.231 208
	2330.00	0.013 03		4027.30	0.012 33		0.6534	0.817 238
	657.466	0.052 27		1144.96	0.049 08		. . .	
	. . .			. . .			0.1776	1.000 00
	214.004	1.000 00		376.954	1.000 00		. . .	
	. . .			. . .		*p*	1.0000	1.000 00
	77.6064	1.000 00		138.070	1.000 00			
	. . .			. . .				
	30.6395	1.000 00		54.9540	1.000 00			
	. . .			. . .				
	12.8156	1.000 00		23.1650	1.000 00			
	. . .			. . .				
	3.927 14	1.000 00		7.376 88	1.000 00			
	. . .			. . .				
	1.452 21	1.000 00		2.923 69	1.000 00			
	. . .			. . .				
	0.257 644	1.000 00		0.650 663	1.000 00			
	. . .			. . .				
	0.094 404	1.000 00		0.232 877	1.000 00			
	. . .			. . .				
p	337.495	0.003 54	*p*	660.901	0.002 99			
	78.6871	0.027 54		157.219	0.023 64			
	24.9351	0.116 49		50.0639	0.105 89			
	9.215 15	0.293 30		18.6119	0.285 67			
	. . .			. . .				
	3.615 26	1.000 00		7.436 92	1.000 00			
	. . .			. . .				
	1.451 99	1.000 00		3.088 57	1.000 00			
	. . .			. . .				
	0.503 992	1.000 00		1.102 67	1.000 00			
	. . .			. . .				
	0.186 040	1.000 00		0.414 763	1.000 00			
	. . .			. . .				
	0.065 432	1.000 00		0.145 449	1.000 00			
	. . .			. . .				
d	0.25	1.000 00	*d*	0.263	1.000 00			
	. . .			. . .				
	0.75	1.000 00		0.950	1.000 00			

TABLE II. The fit of the potential function for the self-consistent-field (SCF) Ar^+-Si potential-energy curve.

Internuclear separation (Å)	Potential functions (eV) SCF[a]	Base function[b]	CP[c]	Fitted function[d]	Residual[e]
0.200	5524.9750[f]	5474.7984	−50.1766	5524.9750	0.0000
0.203	5366.5450	5324.7689	−41.7761	5366.5450	0.0000
0.207	5164.9430	5133.5581	−31.3849	5164.9430	0.0000
0.210	5020.5970	4996.4137	−24.1833	5020.5970	0.0000
0.213	4881.8250	4864.3513	−17.4737	4881.8250	0.0000
0.217	4705.0280	4695.7575	−9.2705	4705.0280	0.0000
0.220	4578.2940	4574.6372	−3.6568	4578.2940	0.0000
0.230	4189.1470	4201.0753	11.9283	4189.1470	0.0000
0.240	3845.6850	3868.8196	23.1346	3845.6850	0.0000
0.250	3541.6330	3572.1416	30.5086	3541.6330	0.0000
0.260	3271.6920	3306.2593	34.5673	3271.6920	0.0000
0.270	3031.3720	3067.1557	35.7837	3031.3720	0.0000
0.280	2816.8410	2851.4376	34.5966	2816.8410	0.0000
0.290	2624.8090	2656.2233	31.4143	2624.8090	0.0000
0.300	2452.4240	2479.0538	26.6298	2452.4240	0.0000
0.310	2297.1780	2317.8212	20.6432	2297.1780	0.0000
0.320	2157.7800	2170.7110	12.9310	2157.7800	0.0000
0.330	2028.8610	2036.1548	7.2938	2028.8610	0.0000
0.340	1909.4720	...	...	1909.4720	0.0000
0.350	1791.6940	...	...	1791.6940	0.0000
0.360	1677.7010	...	...	1677.7010	0.0000
0.370	1570.3740	...	...	1570.3740	0.0000
0.380	1470.1270	...	...	1470.1270	0.0000
0.390	1376.7990	...	...	1376.7990	0.0000
0.400	1290.0690	...	...	1290.0690	0.0000
0.420	1134.8550	...	...	1134.8550	0.0000
0.440	1001.3170	961.0811	−40.2358	1001.3169	−0.0001
0.450	941.7162	915.0575	−26.6591	941.7166	0.0004
0.470	835.0968	829.5165	−5.5801	835.0967	−0.0001
0.480	787.4402	789.7932	2.3535	787.4397	−0.0005
0.500	702.0038	715.9622	13.9581	702.0041	0.0003
0.520	628.0732	649.0330	20.9575	628.0754	0.0022
0.540	563.9253	588.3604	24.4403	563.9201	−0.0052
0.550	535.0373	560.1854	25.1454	535.0399	0.0026
0.570	482.8672	507.8184	24.9501	482.8683	0.0011
0.600	416.5320	438.3020	21.7705	416.5315	−0.0005
0.620	378.8974	397.3289	18.4319	378.8970	−0.0004
0.650	330.4290	342.9376	12.5083	330.4293	0.0003
0.670	302.5399	310.8793	8.3391	302.5402	0.0003
0.700	266.0987	268.3223	2.2239	266.0984	−0.0003
0.720	244.8225	243.2392	−1.5829	244.8221	−0.0004
0.750	216.6498	209.9416	−6.7082	216.6498	0.0000
0.770	199.9969	190.3160	−9.6814	199.9974	0.0005
0.800	177.7010	164.2632	−13.4381	177.7013	0.0003
0.820	164.3785	148.9076	−15.4708	164.3784	−0.0001
0.850	146.3497	128.5233	−17.8259	146.3492	−0.0005
0.870	135.4598	116.5088	−18.9506	135.4594	−0.0004
0.900	120.5753	100.5596	−20.0160	120.5756	0.0003
0.920	111.5072	91.1592	−20.3486	111.5078	0.0006
0.950	99.0400	78.6802	−20.3602	99.0404	0.0003
0.970	91.4202	71.3250	−20.0949	91.4200	−0.0003
1.000	80.9412	61.5612	−19.3792	80.9404	−0.0008
1.050	65.7839	48.1669	−17.6174	65.7843	0.0004
1.100	53.1902	37.6869	−15.5038	53.1907	0.0005
1.150	42.8123	29.4871	−13.3243	42.8114	−0.0010
1.200	34.3184	23.0714	−11.2479	34.3193	0.0009
1.250	27.4016	18.0516	−9.3495	27.4011	−0.0005
1.300	21.7894	14.1240	−7.6656	21.7896	0.0002
1.350	17.2476	11.0509	−6.1966	17.2475	0.0000

TABLE II. (*Continued*).

Internuclear separation (Å)	Potential functions (eV) SCF[a]	Base function[b]	CP[c]	Fitted function[d]	Residual[e]
1.400	13.5788	8.6465	−4.9324	13.5789	0.0000
1.450	10.6201	6.7652	−3.8549	10.6201	0.0000

[a]Hartree-Fock self-consistent-field potential.
[b]The base function to which the SCF potential is fitted is a Molière function at $r \leq 0.330$ Å and a Born-Mayer function at $r \geq 0.440$ Å.
[c]Chebyshev-polynomial (CP) contribution.
[d]Born-Mayer–Chebyshev polynomial.
[e]Fitted function–SCF.
[f]Absolute energy = −614.090 95 hartrees. Energy at internuclear separation 100 Å = −817.128 35 hartrees.

For the Ar^+-Si potential, however, the correlation energy was found to be roughly constant for the full range of interatomic separations considered, indicating that the self-consistent-field (SCF) description of the system provides an adequate calculated potential-energy surface. In all these calculations, the ground-state potential-energy surface was followed throughout, i.e., the $^1A_1$ states for Si_2H_6 and SiH_3Ar^+. For the Si-Si potential, an avoided crossing in the region 1350–800 eV made convergence of the calculations difficult so that we have fitted across this region having very few points. The high-energy region of the Si-Ar^+ potential also contained avoided crossings, but points could still be obtained because the SCF calculations did converge. These observations suggest a possible need for multireference CI calculations, but such refinements would not be expected to significantly alter the results.

All the electronic-structure calculations were performed using the Cambridge Analytic Derivatives Package (CADPAC),[96] and the SDCI calculations were performed using the CI program of Saxe *et al.*[97] interfaced to CADPAC.

The Si-Si and Ar^+-Si potentials were fitted to a Born-Mayer function at low energy and a Molière function at high energy, as described in our previous paper, using routines from the Numerical Analysis Group library[98] NAG Mark 11. The residuals were fitted to Chebyshev polynomials of the first type[99] so that the maximum error between the fitted function and the calculated data points was less than 0.1 eV (see Tables II and III). At low ener-

TABLE III. The fit of the potential function for the SDCI Si-Si potential-energy curve.

Internuclear separation (Å)	SDCI[a]	Potential functions (eV) Base function[b]	CP[c]	Fitted function[d]	Residual[e]
0.300	1916.2200[f]	1899.2480	−16.9720	1916.2200	0.0000
0.320	1666.3410	1662.3255	−4.0155	1666.3410	0.0000
0.350	1373.6910	1377.1707	3.4797	1373.6910	0.0000
0.450	796.5832	794.3918	−2.1914	796.5832	0.0000
0.470	707.1355	719.3739	12.2384	707.1355	0.0000
0.500	591.5873	623.1438	31.5565	591.5873	0.0000
0.550	441.6504	. . .	. . .	441.6504	0.0000
0.600	337.0257	327.3642	−9.6615	337.0257	0.0000
0.650	260.5732	263.4351	2.8618	260.5733	0.0001
0.700	204.8009	211.9904	7.1896	204.8007	−0.0002
0.750	163.5368	170.5920	7.0550	163.5370	0.0002
0.800	132.5646	137.2780	4.7134	132.5647	0.0001
0.850	108.9442	110.4698	1.5260	108.9438	−0.0004
0.900	90.5883	88.8968	−1.6918	90.5886	0.0003
1.000	64.1227	57.5667	−6.5560	64.1226	−0.0001
1.100	45.6898	37.2783	−8.4115	45.6898	0.0000
1.200	31.7548	24.1402	−7.6146	31.7548	0.0000
1.300	20.9415	15.6324	−5.3091	20.9415	0.0000
1.400	12.7084	10.1230	−2.5854	12.7084	0.0000

[a]Configuration interaction potential.
[b]The base function to which the SDCI potential is fitted is a Molière function at $r \leq 0.500$ Å and a Born-Mayer function at $r \geq 0.600$ Å.
[c]Chebyshev polynomial contribution.
[d]Born-Mayer–Chebyshev polynomial.
[e]Fitted function–SDCI.
[f]Absolute energy = −511.205 84 hartrees. Energy at internuclear 100 Å = −581.628 06 hartrees.

TABLE IV. Potential parameters for the SCF Ar^+-Si potential. Numbers in square brackets are powers of ten.

V (eV)	Molière[a]–CP	CP	$A\exp(-Br)$–CP	CP
Range (bohr)	$0.378<r<0.624$	$0.624<r<0.831$	$0.831<r<2.740$	$2.740<r<3.780$
a_{12} (bohr)	0.240 38	⋯	⋯	⋯
A (hartree)	⋯	⋯	306.0	⋯
B ($bohr^{-1}$)	⋯	⋯	2.5967	⋯
CP order	18	16	18	6
CP limits (bohr)	0.378 to 0.624	0.605 to 0.850	0.831 to 2.740	1.740 to 3.780
CP coefficients	0.513 30[0]	0.109 34[3]	−0.468 75[0]	0.254 28[0]
	0.846 11[0]	−0.223 74[2]	−0.108 68[0]	−0.176 71[0]
	−0.105 66[1]	0.230 77[1]	0.967 97[−1]	0.571 73[−1]
	0.190 99[0]	0.170 89[−1]	0.404 84[0]	−0.147 25[−1]
	−0.389 49[−2]	−0.425 10^{−1}	−0.534 70[0]	0.108 26[−1]
	0.804 57[−2]	0.217 94[−1]	0.330 91[0]	−0.370 67[−2]
	0.920 69[−2]	0.337 86[−1]	−0.128 98[0]	⋯
	0.815 70[−2]	−0.319 70[−1]	0.376 99[−1]	⋯
	0.676 31[−2]	−0.229 31[−1]	−0.108 49[−1]	⋯
	0.438 49[−2]	0.164 99[−2]	0.253 03[−2]	⋯
	0.198 55[−2]	0.826 94[−3]	0.125 60[−2]	⋯
	0.118 99[−3]	0.417 18[−1]	0.152 96[−3]	⋯
	−0.927 92[−3]	0.153 41[−1]	−0.169 00[−3]	⋯
	−0.119 31[−2]	−0.185 65[−2]	0.839 09[−3]	⋯
	0.959 54[−3]	−0.851 01[−2]	0.602 27[−3]	⋯
	−0.555 23[−3]	−0.189 28[−1]	−0.102 54[−4]	⋯
	−0.217 14[−3]	⋯	0.274 15[−3]	⋯
	−0.597 50[−4]	⋯	0.202 30[−3]	⋯
3.780 bohrs $<r<\infty$	$V=0$			

[a]The Molière potential function is of the form $V(r_{12})=(Z_1Z_2/r_{12})\Phi(r_{12}/a_{12})$, where $\Phi(x)=0.35\exp(-0.3x)+0.55\exp(-1.2x)+0.10\exp(-6.0x)$.

gy the Si-Si potential was connected to the two-body part of the Stillinger-Weber potential by means of a Chebyshev polynomial, while the Ar^+-Si potential was set to zero at the separation where the electronic-structure potential crosses 0 (i.e., 3.78 bohrs). The final Si-Si and Ar^+-Si potentials are given in Tables IV and V.

A range of alternative repulsive potentials was also used in the simulations. Apart from our new potentials, the Abrahamson[78] potentials of Born-Mayer form, the universal potentials of Biersack and Ziegler,[100] the

TABLE V. Potential parameters for the SDCI Si-Si potential. Numbers in square brackets are powers of ten.

V (eV)	Molière[a]–CP	CP	$A\exp(-Br)$–CP	CP
Range (bohr)	$0.567<r<0.945$	$0.945<r<1.339$	$1.339<r<2.457$	$2.457<r<2.844$
a_{12} (bohr)	0.236 94	⋯	⋯	⋯
A (hartree)	⋯	⋯	163.1	⋯
B ($bohr^{-1}$)	⋯	⋯	2.2994	⋯
CP order	6	9	10	9
CP limits (bohr)	0.567 to 0.945	0.888 to 1.228	1.339 to 2.457	2.268 to 3.024
CP coefficients	0.210 22[0]	0.331 11[2]	−0.199 21[0]	0.114 32[1]
	0.611 38[0]	−0.811 54[1]	−0.111 32[0]	−0.494 48[0]
	0.294 54[0]	0.117 55[1]	0.188 94[−1]	0.964 45[−1]
	0.366 70[0]	−0.630 27[−1]	0.194 08[0]	−0.661 90[−2]
	−0.131 67[0]	0.141 64[−1]	−0.132 60[0]	−0.387 27[−2]
	−0.863 92[−1]	−0.293 64[−1]	0.432 62[−1]	0.119 19[−5]
	⋯	0.796 28[−1]	−0.109 46[−1]	0.298 92[−2]
	⋯	0.246 12[−2]	0.372 86[−2]	0.288 35[−4]
	⋯	−0.435 99[−1]	−0.774 62[−3]	−0.129 43[−2]
	⋯	⋯	0.275 24[−3]	⋯
3.780 bohrs $<r<\infty$	$V=$ Stillinger-Weber potential			

[a]The Molière potential function is of the form $V(r_{12})=(Z_1Z_2/r_{12})\Phi(r_{12}/a_{12})$, where $\Phi(x)=0.35\exp(-0.3x)+0.55\exp(-1.2x)+0.10\exp(-6.0x)$.

TABLE VI. Comparison of various Ar^+-Si potentials.

Internuclear Separation (Å)	SCF[a] (eV)	Smith[b] (eV)	Moliére[c] (eV)	Universal[d] (eV)	Abrahamson[e] (eV)
0.200	5524.97	5707.63	4392.95	5065.23	2859.99
0.220	4578.29	4731.71	3633.36	4175.89	2657.92
0.250	3541.63	3648.78	2798.99	3188.02	2381.27
0.280	2816.84	2877.33	2207.28	2481.70	2133.41
0.300	2452.42	2482.11	1904.32	2119.29	1982.68
0.330	2028.86	2007.40	1546.49	1692.24	1776.31
0.350	1791.69	1753.19	1356.36	1466.67	1650.81
0.380	1470.13	1443.56	1124.75	1194.40	1478.98
0.400	1290.07	1275.24	998.21	1047.40	1374.49
0.420	1134.85	1131.29	889.26	922.20	1277.37
0.450	941.72	952.17	752.36	767.20	1144.42
0.480	787.44	807.81	640.59	643.08	1025.30
0.500	702.00	726.82	577.22	573.88	952.86
0.520	628.07	655.82	521.23	513.56	885.53
0.550	535.04	564.80	448.88	436.88	793.36
0.570	482.87	512.70	407.18	393.42	737.31
0.600	416.53	445.06	352.77	337.58	660.56
0.650	330.43	354.43	279.59	264.20	550.00
0.670	302.54	324.32	255.26	240.28	511.14
0.700	266.10	284.47	223.11	209.04	457.93
0.750	216.65	229.64	179.06	166.97	381.28
0.800	177.70	186.14	144.40	134.49	317.46
0.850	146.35	151.33	116.94	109.12	264.32
0.900	120.58	123.29	95.04	89.12	220.08
0.950	99.04	100.59	77.49	73.21	183.24
1.000	80.94	82.16	63.36	60.46	152.57
1.100	53.19	54.92	42.67	41.83	105.77
1.200	34.32	36.77	28.98	29.43	73.32
1.300	21.79	24.64	19.82	21.01	50.83
1.400	13.58	16.51	13.64	15.20	35.24
1.500	8.24	11.07	9.43	11.13	24.43
1.700	2.58	4.98	4.57	6.18	11.74
1.900	0.32	2.24	2.24	3.56	5.64

[a]Hartree-Fock-self-consistent field potential.
[b]G. L. Smith (Ref. 76) using the modified Wedepohl method (Refs. 79–81).
[c]Molière potential (Refs. 101 and 102): $Z_1=18$; $Z_2=14$; $a_{12}=0.100\,06$ Å.
[d]Universal Potential (Ref. 100): $Z_1=18$; $Z_2=14$; $a_{12}=0.123\,97$ Å.
[e]Abrahamson Potential (Ref. 78): $A=5.95$ keV; $B=3.66$ Å.

Molière potentials[101] with screening lengths calculated using the formula of O'Connor and Biersack,[102] and the Smith[76] potentials were also used, i.e., pairs of potentials were constructed from each functional form, the Si-Si potential was splined to the Stillinger-Weber potential, and the pair was tested in the classical-trajectory calculations. Figures 1 and 2 and Tables VI and VII show a comparison of the variously proposed Ar^+-Si and Si-Si potentials over a range of interatomic separations.

III. THE CLASSICAL-TRAJECTORY CALCULATIONS

The classical-trajectory method was used to simulate the collision of an ion or molecule with a semi-infinite solid. The first priority in such calculations is to choose the most suitable coordinate system in which to describe the dynamics. Unlike atom-diatom scattering,[103] no benefit is to be gained by choosing a barycentric coordinate because the position vector of the center of mass is essentially unchanged throughout the calculation. The position vectors of the atoms are consequently best described by reference to a Cartesian set of axes defined with the Z axis fixed in space in the [001] direction (i.e., normal to the surface and directed out of the solid), and with the X and Y axes lying in the plane of the solid surface along suitable symmetry directions. The coordinate system for the simulation of Ar^+-Si(001) is shown in Fig. 3.

The sampling scheme adopted is that of Harrison Jr. *et al.*[55,77] Provided that the microcrystallite is derived from a monocrystal with the solid atoms placed on the lattice sites with zero momentum, each impact point on the target surface may be mapped onto an equivalent point within an irreducible symmetry zone. By sampling impact points uniformly over this irreducible symmetry zone, an ensemble of trajectories is generated which is representative of the set of all possible trajectories which may be generated from a given ion initial momentum vec-

TABLE VII. Comparison of various Si-Si potentials.

Internuclear separation (Å)	SDCI[a] (eV)	Smith[b] (eV)	Moliére[c] (eV)	Universal[d] (eV)	Abrahamson[e] (eV)
0.300	1916.22	2066.18	1513.93	1712.65	1670.52
0.320	1666.34	1769.57	1316.53	1474.39	1551.31
0.350	1373.69	1417.36	1080.13	1190.11	1388.25
0.450	796.58	731.07	601.48	626.97	958.74
0.470	707.14	648.51	540.46	557.66	890.32
0.500	591.59	545.63	462.49	470.47	796.74
0.550	441.65	416.34	360.52	359.24	662.12
0.600	337.03	324.07	284.04	278.40	550.24
0.650	260.57	256.80	225.70	218.49	457.26
0.700	204.80	206.74	180.58	173.36	380.00
0.750	163.54	168.78	145.32	138.86	315.79
0.800	132.56	139.47	117.52	112.16	262.43
0.850	108.94	116.46	95.43	91.25	218.09
0.900	90.59	98.12	77.78	74.73	181.24
1.000	64.12	71.13	52.14	50.97	125.16
1.100	45.69	52.67	35.32	35.45	86.44
1.200	31.75	39.57	24.12	25.06	59.70
1.300	20.94	30.02	16.59	17.98	41.23
1.400	12.71	22.93	11.48	13.07	28.47

[a]Configuration interaction potential.
[b]G. L. Smith (Ref. 76) using the modified Wedepohl method (Refs. 79–81).
[c]Molière potential (Refs. 101 and 102): $Z_1=14$; $Z_2=14$; $a_{12}=0.101\,98$ Å.
[d]Universal Potential (Ref. 100): $Z_1=14$; $Z_2=14$; $a_{12}=0.127\,66$ Å.
[e]Abrahamson Potential (Ref. 78): $A=5.07$ keV; $B=3.70$ Å.

tor. Tests with increasing ensemble size indicate that sputtering yields have converged to within 5% after 150–250 individual trajectories. Similarly, Harrison Jr. finds that different ensembles of 80–100 trajectories chosen in this way reproduce the calculated sputtering yield to better than 10%.[104] Figure 4 shows the irreducible symmetry zone and the sample impact points for a normally incident ion on the Si(001) unreconstructed and (2×1) reconstructed surfaces.

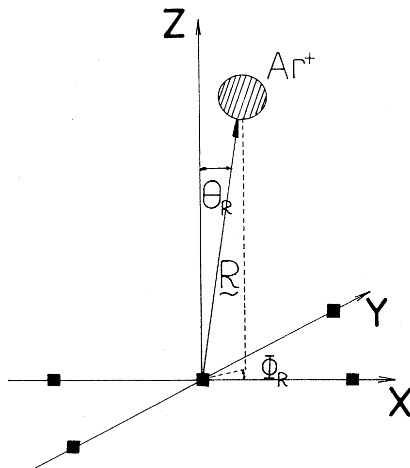

FIG. 3. The coordinate system for the $Ar^+ + Si(001)$ calculations. The X axis lies in the (110) direction, the Y axis in the $(1\bar{1}0)$ direction, and the Z axis perpendicular to and out of the surface.

Classical-trajectory calculations have been performed on the sputtering of the Si(001) surface by Ar^+ ions using the new, and some of the previously proposed, potentials. It was found that a minimum of eight layers of atoms was required to develop the bulk yield at all the energies considered. Two sets of calculations were performed, one on the bulk terminated (001) surface, the other on a model of the (2×1) reconstructed surface. For the calculations on the unreconstructed surface, all of the atoms were initially placed at the bulk position vectors of the solid. A microcrystallite of 842 atoms was found to ensure adequate containment, except at 200 eV where a 442-atom micro-

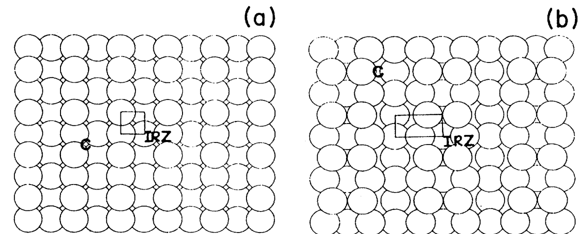

FIG. 4. Sampling over the irreducible symmetry zone of the Si(001) (a) unreconstructed and (b) (2×1) reconstructed surfaces. Each point within the rectangles denoting the irreducible symmetry zones corresponds to one of the impact points of the argon ion in the set of trajectories. IRZ, irreducible symmetry zone; C, channel.

crystallite proved to be sufficient. For the calculations on the reconstructed surface, bulk position vectors were adopted for the atoms below layer 4. The position vectors of the upper layers were set to those of Abraham and Batra,[63] which describe the perfect (2×1) reconstructed surface. A 1058-atom lattice was adopted at energies of 1000 eV and above, with smaller lattices being used at lower energies. The employment of larger lattices to improve the lattice containment[105] did not significantly alter the calculated sputtering yield. A total of 144 trajectories was run sampling over the irreducible symmetry zone of the unreconstructed surface, while for the reconstructed surface calculations 288 were run at low energies and 190 at higher energies. These calculations proved to be very expensive in computer time because the third-body forces are very costly to evaluate. One trajectory using a 1058-atom lattice took an average of 40 central-processing-unit (CPU) minutes on a CONVEX C1 vector computer and 20 CPU minutes on an IBM 3084 computer. Integration of Hamilton's equations of motion was carried out using the variable-order, variable-step predictor-corrector integrator D02QAF from the NAG (Ref. 98) subroutine library.

IV. RESULTS AND DISCUSSION

Figure 5 and Table VIII show the variation of the calculated sputtering yields with beam kinetic energy. As for Ar^+-Cu(001),[89] the calculated sputtering yields are found to be very sensitive to the choice of potential. For the calculations on the unreconstructed Si(001) surface, all the potentials give a sputtering-yield curve which, when compared to experiment, is initially too low and then rises too steeply at larger kinetic energies. A number of experimental sputtering-yield curves for the Ar^+-ion sputtering of silicon have been published.[83,106–118] However, some studies[106,111,112] were performed before ultrahigh-vacuum techniques became available and these sputtering yields have since been shown to be too low,[110] while other determinations[83,109] have been at ion-beam energies greater than those considered in these simulations. The experimental sputtering yields given in the Table VIII and Fig. 5 are those of Zalm,[110] which are in agreement with earlier determinations by Coburn[107] and Harper *et al.*[114] One difficulty in comparing the calculated sputterings yields with experiment is that Zalm's results were obtained using a total ion fluence of 10^{18} cm^{-2}. Blank and Wittmaack[83] and Kempf[84] find that the sputtering yield for Ar^+-ion sputtering of silicon rises to some steady-state value with increasing ion fluence as Ar is implanted in the surface. In addition, the silicon surface is amorphized at ion doses as low as 0.1 ion per surface atom.[119] Since each trajectory in these calculations begins with an undamaged surface, a direct comparison with these experiments is not possible. Unfortunately, no low-dose sputtering yields for Ar^+-Si(001) are currently available. However, Zalm's results do provide a limit above which any predicted sputtering yield must be in error.

Figure 5 and Table VIII also give the calculated variation of the sputtering yield with ion-beam kinetic energy

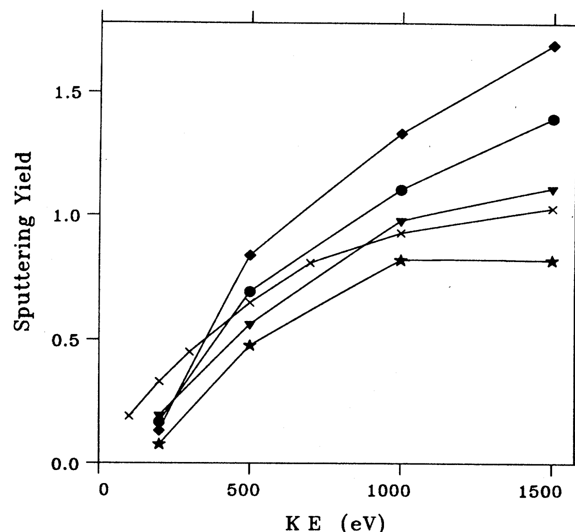

FIG. 5. Experimental and calculated Ar^++Si(001) sputtering yields. ×, Experiment (Ref. 110) (steady-state yield); ●, the SDCI and SCF potentials (unreconstructed surface); ♦, the Smith modified Wedepohl potentials (unreconstructed surface); ▼, the Biersack-Ziegler universal potentials (unreconstructed surface); ★, the SDCI and SCF potentials (reconstructed surface).

for the reconstructed Si(001) surface when using the electronic-structure potentials. The predicted yields are very different from those for the unreconstructed surface, and, as expected, lie consistently below experiment. This large change in the calculated sputtering yield on surface reconstruction is well predicted by theory. Using the Stillinger-Weber potential,[43] the Si(001) reconstructed surface has a calculated increased surface binding energy of 0.83 eV per atom over the unreconstructed surface. Both Sigmund's formula[120] and previous classical-trajectory calculations by Harrison, Jr. and Webb[121] and Garrison[30] predict that the sputtering yield should decrease with an increase in the surface binding energy. From Fig. 5 it appears that the Smith potential might give a better agreement with experiment when using the reconstructed surface than the new potential. However, as discussed above, comparison with experiment is not really valid till low-dose data become available.

Table IX presents the calculated-layer sputtering-yield ratios at 500 and 1500 eV for the reconstructed and unreconstructed surfaces when using the new Si-Si and Ar^+-Si potentials. The quantity L_n is defined as the ratio of the sputtering yield arising from layer n to the total sputtering yield. In this case, the values are very different from that observed for metals where $L_1>0.85$, $L_2\lesssim0.13$, and $L_3\lesssim0.02$, with a negligible contribution to the sputtering yield from the lower layers.[28,105,121–124] The reason for this difference is found in the very open structure of the Si lattice: the first-layer atoms are sufficiently separated for there to be room for lower-layer atoms to eject without undergoing strong collisions with first-layer atoms. For metals such as copper, second-layer atoms generally only eject through vacancies in the surface from

TABLE VIII. Calculated etching yields for Ar^+-Si(001) for various Ar^+-Si and Si-Si potentials.

Beam kinetic energy (eV)	Experiment (Zalm)[a]	Universal potential[b]	Smith potential[b]	SDCI/SCF potential[b]	SDCI/SCF potential[c]
100	0.19±0.03	...	...	...	...
200	0.33±0.03	0.19±0.04	0.32±0.03	0.17±0.04	0.08±0.02
300	0.45±0.04	...	...	...	...
500	0.65±0.05	0.56±0.10	0.84±0.11	0.70±0.08	0.48±0.05
700	0.81±0.05	...	...	...	...
1000	0.93±0.06	0.98±0.14	1.33±0.15	1.10±0.12	0.82±0.08
1500	1.03±0.06	1.11±0.14	1.69±0.18	1.40±0.19	0.82±0.08

[a]Steady-state yield.
[b]Simulation on the unreconstructed surface.
[c]Simulation on the (2×1) reconstructed surface using the position vectors of Abraham and Batra (Ref. 63).

where a first-layer atom has been displaced.[123]

On surface reconstruction, the layer ejection yields change appreciably. The absolute sputtering yield of the reconstructed first layer is about 40% of that of the unreconstructed first layer. This is because of the increased surface binding energy of each first-layer atom as described above. The sputtering yield of the second layer is not so severely affected, decreasing only to 70% of its former value. The sputtering yields of the lower layers are essentially unchanged within statistical error. In consequence the first- and second-layer yield ratios become very similar for the reconstructed surface.

Figure 6 gives the atoms per single ion (ASI) distributions for the unreconstructed and reconstructed surfaces

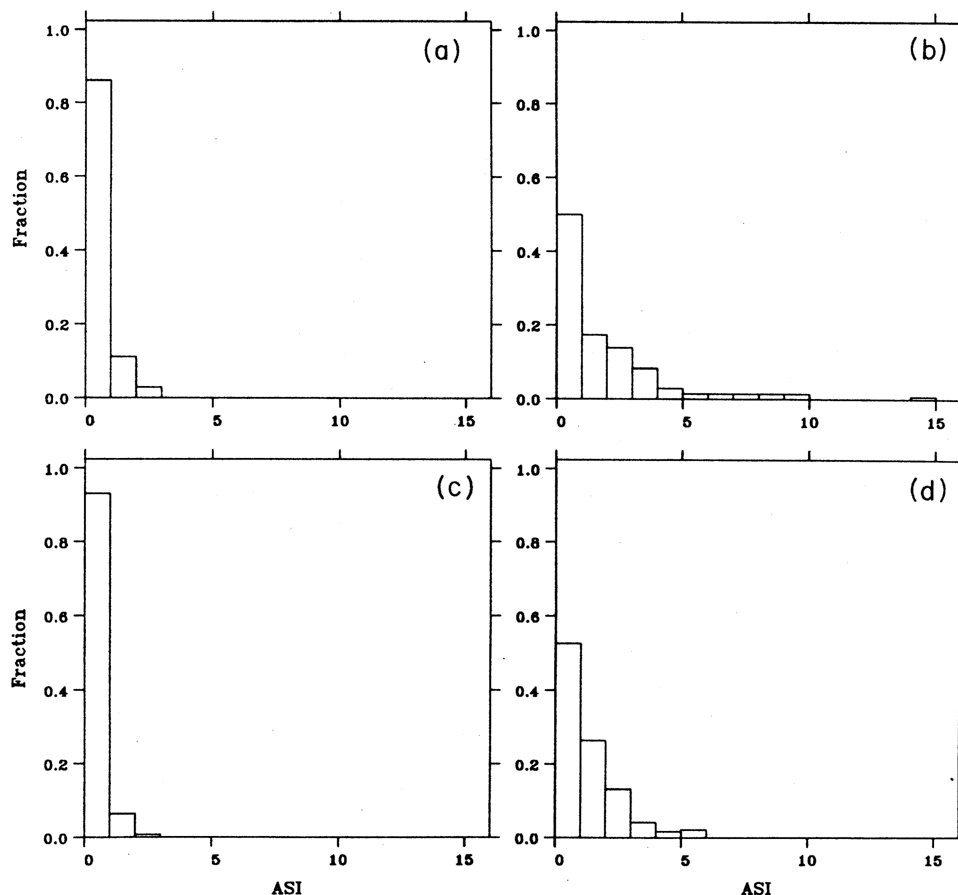

FIG. 6. A comparison of the atom per single ion (ASI) distributions for the unreconstructed and reconstructed surfaces at different energies. (a) 200 eV unreconstructed surface; (b) 1500 eV unreconstructed surface; (c) 200 eV reconstructed surface; (d) 1500 eV reconstructed surface.

TABLE IX. Layer ejection ratios for the SDCI-SCF potentials.

KE (eV)	L_1	L_2	L_3	L_4
500[a]	0.46	0.26	0.19	0.09
500[b]	0.36	0.34	0.24	0.00
1500[a]	0.51	0.23	0.14	0.07
1500[b]	0.36	0.28	0.22	0.10

[a]Unreconstructed surface.
[b]Reconstructed surface.

at two different energies using the new Ar$^+$-Si and Si-Si potentials. The effect of the surface reconstruction is evident in reducing the number of high-yield ejection events. The large number of zero-yield trajectories emphasizes the importance of the channel in the Si(001) face. Figure 7 plots the sputtering yield of individual trajectories at 1500 eV against the impact point of the ion within the irreducible symmetry zone. For the unreconstructed surface, the channeling of the ion is evident from the zero ASI's at the center of each irreducible symmetry zone. Other zero ASI's are to be found where the ion is able to penetrate to the fourth layer without undergoing any strong collisions confirming that sputtering mechanisms, as for metals,[28] are predominantly confined to the surface layers. On surface reconstruction, half the channels are closed by the surface dimers. However, the large holes left in the surface by this process, and the increased size of the channel in the uppermost four layers, provides another reason for the decreased sputtering yield: a large proportion of the incident ions undergo a primary impact with the third or fourth layers, thus causing radiation damage without sputtering.

It is expected that the calculated sputtering yields for the (2×1) reconstructed Si(001) surface will compare favorably with low-dose experiments when such data become available. However, some uncertainties do remain within the model. Firstly, the exact nature of the surface reconstruction of the Si(001) surface is unknown. The Abraham-Batra structure is a close approximation, but the omission of the dimer buckling and twisting and the surface defects may influence the calculated sputtering yield. Further, while the Stillinger-Weber potential provides a reasonable representation of the low-energy silicon potential-energy surface, it is unknown how important the deficiencies described in the introduction may be. The Brenner-Garrison potential gives a better description of the potential-energy surface for small displacements from the perfect diamond lattice, but there is no evidence as to which potential is best suited for sputtering calculations. A further source of error is the omission of electronic effects. Since dimer buckling involves a charge transfer of $0.4e$,[59] it is possible that charge transfers may be important in describing low-energy collisions within the solid. This effect is more important here than within a metal, since electronic perturbations will be more localized within silicon. Energy losses through phonon modes have additionally been neglected.

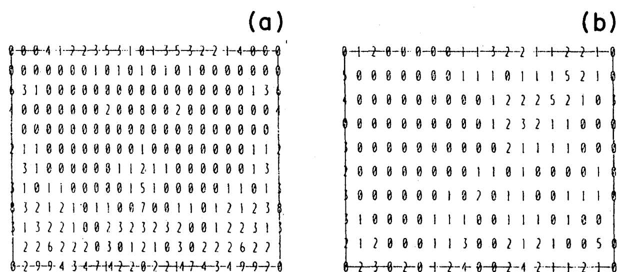

FIG. 7. Channeling in the Si(001) surface at 1500 eV. Each plotted number corresponds to the ASI of the trajectory whose impact point is at the center of the number. (a) The unreconstructed surface; (b) the reconstructed surface. The data for the unreconstructed surface cover two irreducible symmetry zones to enable a direct comparison with the data for the reconstructed surface.

We now discuss parameters we have calculated using the new Ar$^+$-Si and Si-Si potentials which are amenable to experimental investigation. The sputtering yield for Ar$^+$ bombardment of silicon is very low, making it difficult to generate statistically viable distribution functions. Since the only effect of increasing the beam kinetic energy is expected to be an extension of the tail of the kinetic-energy distribution to higher energies,[120,125–127] the data for the four energies have been combined. Figure 8 gives the kinetic-energy distributions for the sputtered atoms. The general shape of the distributions are of the usual sputtering type which has been observed for other systems, both in experiment[125,128–131] and in theoretical calculations.[27,77,105,108,121–123,125–129,132,133] Unfortunately, the only available kinetic-energy distribution data for Si do not extend to energies below 20 eV.[131]

For both the unreconstructed and reconstructed surfaces, the maximum in the kinetic-energy distribution is observed to be at 4–6 eV (Fig. 8). Statistical theories[120,125–127] predict that the maximum should be near $U_s/2$, where U_s is the surface binding energy. Conventionally, this has been taken to be at half the sublimation energy of silicon, i.e., at 2.2 eV. However, recent experiments indicate that the maximum might be expected to be found at about $0.7-0.8U_s$. This is in agreement with calculations by Garrison *et al.*[129,133] on the Ar$^+$ sputtering of rhodium. The energy distributions obtained here peak at an energy greater than this, but it is uncertain whether this is statistically significant. On surface reconstruction it appears that there might be a shift in the maximum of the distribution to higher energy. This would be in agreement with statistical theories, since the surface binding energy has increased by 0.83 eV per surface atom, but again it is uncertain whether the shift is statistically significant.

Several experimental studies of the polar-angular distribution of the sputtered atoms exist in the literature,[134–136] but, as for the sputtering-yield experiments, they are performed in the high-dose mode in which the silicon surface is quickly amorphized. It is found that the polar-angle distribution is less than cosine at 500 eV (Ref. 136) and cosine at ion beam energies of 1000 eV and greater.[134–136] The distribution found in the simulations is very different, as might be expected for a crystalline

surface, with a broad maxima at 40°–70°. However, as for the kinetic-energy distributions, the statistics for the individual energies is very poor, and given that experiment indicates that the distribution may change with energy, it is inappropriate to combine the data for the different ion beam kinetic energies.

Very little experimental data are available for the azimuthal angular distribution for the sputtering of silicon. This is because when the surface is amorphized under experimental conditions, the structure in the azimuthal angular distribution is destroyed. Nelson and Mazey[137] have studied the variation of the ion dosage required to amorphize the surface with temperature and find the required dosage for amorphization is 2 orders of magnitude greater at 200° than at room temperature. MacDonald *et al.* have found structure in the azimuthal angular distributions of Ar^+-ion sputtering of Si(001) above a transition temperature of 400±5 °C (Ref. 85) and for Ge(001) above 330°±5 °C.[75,85,86,138,139] These transitions correspond to the annealing of regions of the surface between ion impacts so that the crystallographic structure is retained throughout the experiment. These experiments find maxima at 0°, 90°, 180°, and 270°, where the X and Y axes are defined to lie along the [110] and [$\bar{1}$10] directions, respectively, and the Z axis is normal to, and points out of, the surface.

Figure 9 gives the calculated azimuthal angular distributions for the Ar^+-ion sputtering of both the unreconstructed and (2×1) reconstructed Si(001) surfaces. The calculated distributions are found to be very strongly peaked at 90° intervals. Classical-trajectory calculations on the Ar^+ sputtering of Cu(001) have previously shown a similar structure in the azimuthal distributions.[140] The structure in the distribution has been found to be contained by the atoms sputtered at high energy (> 5 eV) soon after the ion impact. Since each atom in an undamaged Cu(001) surface is surrounded by four neighboring atoms, these structures have been explained by the argument that atoms sputtering before the surface structure is destroyed prefer to eject along a trajectory through the gap between two neighboring atoms rather than directly over a neighboring atom.[140] However, this mechanism cannot apply for the sputtering of silicon for several reasons. Firstly, the maxima in the azimuthal angular distributions would be expected to shift on surface reconstruction if this focusing mechanism was applicable. Secondly, the atoms in the unreconstructed silicon surface are too far apart for a focusing mechanism to operate, and on surface reconstruction only one atom is close enough. Finally, the maxima in the azimuthal distribution are for atoms which do eject directly over their nearest neighbor [i.e., along the ⟨110⟩ directions].

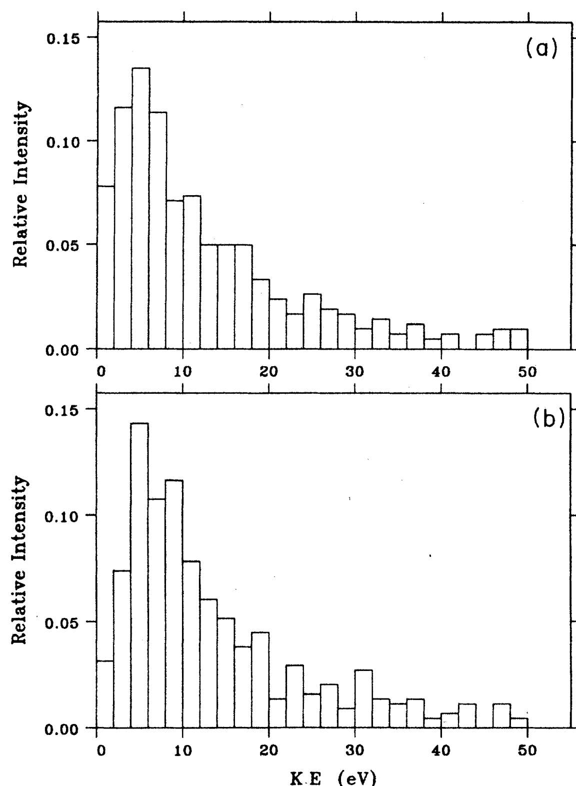

FIG. 8. Histogram of the kinetic-energy distribution of the ejected silicon atoms. The bin size is 2 eV. The data for the four beam kinetic energies have been combined to improve the statistics. (a) The unreconstructed surface; (b) the reconstructed surface.

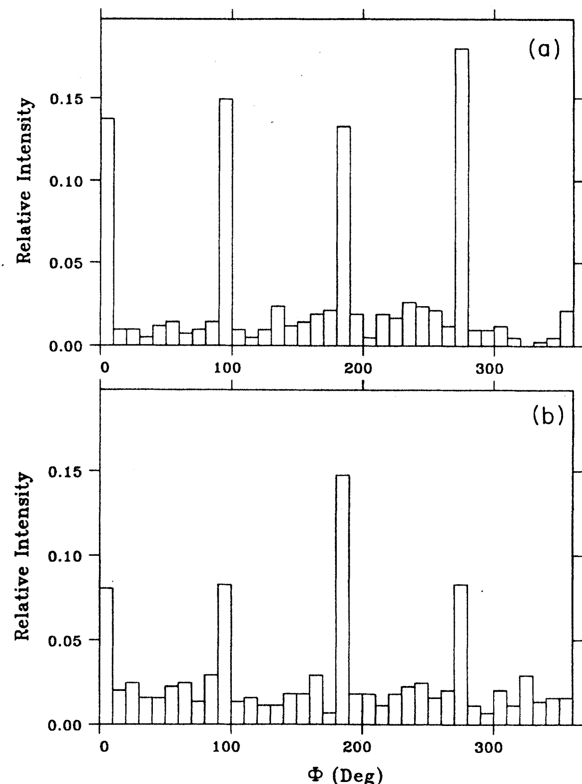

FIG. 9. Histogram of the azimuthal angular distribution of the ejected silicon atoms. The bin size is 10°. The data for the four beam kinetic energies have been combined to improve the statistics. (a) The unreconstructed surface; (b) the reconstructed surface.

A more detailed examination of the azimuthal angular distributions indicates that the structural information is carried by high-energy atoms, which suggests that the lattice structure is an important factor in generating these maxima. Additionally, it is found that atoms ejecting from all of the first four layers contribute to the maxima, emphasizing that the silicon lattice is sufficiently open for atoms to eject from the lower layers without undergoing significant collisions with upper layers. Smith[76] in his previous study of the sputtering of silicon by Ar^+ ions examined the spread of momentum in the initial stages of a trajectory. He found that momentum spread initially along the (110) row of the (first- and second-layer) atoms which contained the target atom. In time, momentum was transferred outwards into neighboring (110) rows of (third- and fourth-layer) atoms and then to the adjacent (110) rows of first- and second-layer atoms. This is confirmed in these simulations. Atoms are found to be ejected at 0°, 90°, 180°, and 270° when an ion impacts very close to or on a row of atoms in the [110] or [$\bar{1}$10] directions. A collision sequence of two or three atoms propagating along the row finally gives rise to an atom ejecting in the appropriate direction. Since the dimer reconstruction is along the [110] direction, surface reconstruction would not be expected to significantly alter this ejection mechanism; hence, the similarity between the two azimuthal angular distributions in Fig. 9. If the ion impact is too far away from a row of atoms, the collision sequence is quickly defocused and any atom sputtered will do so in an essentially random direction. The adoption of a warm lattice, in which the atoms will be displaced from the perfect rows in the zero-temperature lattice, will similarly be expected to defocus the collision sequences and thus considerably broaden the maxima in the calculated azimuthal angular distributions.

One point of contention between experimentalists and theoreticians has been the nature of the formation of clusters. As soon as two or more atoms are sputtered from the solid during a single trajectory, there exists the possibility that a dimer or larger cluster may form. Cluster formation was first detected experimentally by Hönig[141] in 1958 when he observed the formation of Ge_2 dimers while sputtering germanium with rare-gas ions. Since then, clusters containing up to several tens of atoms have been observed in a variety of systems.[29,142–149] The first simulations of cluster formation were by Harrison Jr. and Delaplain[150] for the argon-ion bombardment of a Cu(001) surface. This paper describes the method of detecting cluster formation from sputtered atoms in classical-trajectory calculations and examines the various mechanisms involved.

Classical dynamics simulations on the sputtering of metals have indicated that the vast majority of clusters form via a recombination mechanism above the surface between atoms sputtered in the same collision cascade.[151–157] However, some claims have been made for the ejection of clusters intact from the surface.[158–161] Classical-trajectory calculations in the past have indicated that strongly bonded molecules such as CO and aromatics may be ejected as intact entities. Essentially, weakly bound substances, such as metals where the dimer well depth is generally less than 1 eV,[162] form clusters by a recombination mechanism while strongly bound systems, such as CO whose well depth is 11.1 eV, may be ejected intact. Silicon, with a well depth in the dimer interaction of 2.17 eV, is intermediate between these extremes and might be expected to exhibit both mechanisms.

Experimentally, silicon cluster ions containing up to four Si atoms have been detected in sputtering experiments,[143,161] while Tsong[144] detected cluster ions up to Si_{17}^{n+} in laser desorption studies. However, since the proportion of trajectories which sputter two or more atoms is rather small (Fig. 6), only a few clusters have been detected in these simulations. Of the clusters observed, all the dimers were bound by more than 1 eV, and in both the quadramers, all the interactions between pairs of atoms were binding. Thus it is not anticipated that the difficulties in defining cluster formation will be important, especially as the well depth of the Si_2 interaction is similar in the bulk and gas phase. For the studies using the reconstructed surface, which provides the most realistic initial conditions, only eight dimers and two quadramers were observed. No surface dimers were found to eject as clusters and six of the sputtered dimers were formed by the recombination mechanism. However, the other two clusters were formed between first- and second-layer atoms which were directly bonded within the solid. Examination of these trajectories indicates that in each case the two atoms that eventually comprised the final dimer were within bonding distance throughout the trajectory. A similar situation was found for a pair of atoms within one of the quadramers. However, a definitive statement on the relative importance of these rival cluster-formation mechanisms requires a more extensive study.

V. CONCLUSIONS

The sputtering of the Si(001) surface by Ar^+ ions has been studied using classical-trajectory methods. *Ab initio* calculations have been used to parametrize the Ar^+-Si and the short-range part of the Si-Si interaction, while the silicon binding potential was described by the two- and three-body terms of Stillinger and Weber. It is found that the choice of the potential-energy function to describe the high-energy Si-Si and Ar^+-Si interactions strongly influences the calculated sputtering yield. Unlike previous calculations on metal surfaces, it is essential that the reconstruction of the silicon surface be included in the model. Sputtering yields have been calculated over a range of ion beam kinetic energies which may be compared with low-dose experiments when such data become available. Possible remaining sources of error in the model have been noted. Calculated azimuthal distributions are in agreement with experiment and the mechanisms which give rise to the structure in these distributions have been examined. Some evidence has been found that silicon dimers may be ejected intact from the surface, although most dimers are formed by the recombination mechanism observed in simulations of the sputtering of metals.

ACKNOWLEDGMENTS

We are pleased to acknowledge helpful suggestions on our *ab initio* calculations from Dr. J. E. Rice and Dr. R. D. Amos. Dr. A. Spears (GEC Research Limited) and Dr. T. I. Cox (Royal Signals and Radar Establishment, Malvern) are thanked for their suggestions and encouragement. This work was supported by the Alvey Programme, project ALV/APP/VLSI/010 through United Kingdom Science and Engineering Research Council (SERC) Grant No. GR/D/15836 and the European Economic Community (EEC). The classical-trajectory calculations were performed on the IBM 3084 computer and CONVEX C1 vector computer at University of Cambridge, and the potential calculations were carried out on the Cray Research, Inc. 1S computer at the University of London Computing Center.

[1]S. M. Sze, in *VLSI Technology,* edited by S. M. Sze (McGraw-Hill, New York, 1983).

[2]E. G. Spencer and P. H. Schmidt, J. Vac. Sci. Technol. **8**, S52 (1971).

[3]S. Somekh, J. Vac. Sci. Technol. **13**, 1003 (1976).

[4]C. M. Melliar-Smith, J. Vac. Sci. Technol. **13**, 1008 (1976).

[5]J. A. Bondur, J. Vac. Sci. Technol. **13**, 1023 (1976).

[6]R. E. Lee, J. Vac. Sci. Technol. **16**, 164 (1979).

[7]M. W. Geis, G. A. Lincoln, N. Efremow, and W. J. Piacentini, J. Vac. Sci. Technol. **19**, 1390 (1981).

[8]G. A. Lincoln, M. W. Geis, L. J. Mahoney, A. Chu, B. A. Vojak, K. B. Nichols, W. J. Piacentini, N. Efremow, and W. T. Lindley, J. Vac. Sci. Technol. **20**, 786 (1982).

[9]G. A. Lincoln, M. W. Geis, S. Pang, and N. N. Efremow, J. Vac. Sci. Technol. B **1**, 1043 (1983).

[10]S. W. Pang, G. A. Lincoln, R. W.. McClelland, P. D. DeGraff, M. W. Geis, and W. J. Piacentini, J. Vac. Sci. Technol. B **1**, 1334 (1983).

[11]J. D. Chinn and E. D. Wolf, J. Vac. Sci. Technol. B **3**, 410 (1985).

[12]Y. Ochiai, K. Shihoyama, T. Shiokawa, K. Toyada, A. Masuyama, K. Gamo, and S. Namba, J. Vac. Sci. Technol. B **4**, 333 (1986).

[13]H. F. Winters and J. W. Coburn, Appl. Phys. Lett. **34**, 70 (1979).

[14]M. J. Vasile and F. A. Stevie, J. Appl. Phys. **53**, 3799 (1982).

[15]F. A. Houle, J. Appl. Phys. **60**, 3018 (1986).

[16]J. W. Coburn and H. F. Winters, J. Appl. Phys. **50**, 3189 (1979).

[17]J. W. Coburn and H. F. Winters, J. Vac. Sci. Technol. **16**, 391 (1979).

[18]G. C. Schwartz and P. M. Schaible, J. Vac. Sci. Technol. **16**, 410 (1979).

[19]Y.-Y. Tu, T. J. Chuang, and H. F. Winters, Phys. Rev. B **23**, 823 (1981).

[20]H. F. Winters, J. Vac. Sci. Technol. B **1**, 927 (1983).

[21]D. E. Ibbotson, D. L. Flamm, J. A. Mucha, and V. M. Donnelly, Appl. Phys. Lett. **44**, 1129 (1984).

[22]J. Z. Li, I. Adesida, and E. D. Wolf, Appl. Phys. Lett. **45**, 897 (1984).

[23]J. D. Chinn, I. Adesida,, and E. D. Wolf, J. Vac. Sci. Technol. B **1**, 1028 (1983).

[24]C. J. Mogab, in *VLSI Technology,* edited by S. M. Sze (McGraw-Hill, New York, 1983), Chap. 8.

[25]T. M. Mayer, M. S. Ameen, and D. J. Vitkavage, in *Surface Properties of Electronic Materials (The Chemical Physics of Solid Surfaces and Heterogenous Catalysis),* edited by D. A. King and D. P. Woodruff (Elsevier, Amsterdam, 1988), Vol. 5, Chap. 10.

[26]T. E. Seidel, in *VLSI Technology,* edited by S. M. Sze (McGraw-Hill, New York, 1983), Chap. 6.

[27]C. T. Reimann, K. Walzl, M. El-Maazawi, D. M. Deaven, B. J. Garrison, and N. Winograd, J. Chem. Phys. **89**, 2539 (1988).

[28]D. E. Harrison, Jr., P. W. Kelly, B. J. Garrison, and N. Winograd, Surf. Sci. **76**, 311 (1978).

[29]N. Winograd and B. J. Garrison, Acc. Chem. Res. **13**, 406 (1980).

[30]B. J. Garrison, in *Potential Energy Surfaces and Dynamics Calculations for Chemical Reactions and Molecular Energy Transfer,* edited by D. G. Truhlar (Plenum, New York, 1981), Chap. 36.

[31]D. W. Moon, N. Winograd, and B. J. Garrison, Chem. Phys. Lett. **114**, 237 (1985).

[32]V. A. Eltekov, O. A. Popova, and V. E. Yurasova, Rad. Eff. **83**, 39 (1984).

[33]T. Halicioğlu, Phys. Status Solidi **99**, 347 (1980).

[34]T. Takai, T. Halicioğlu, and W. A. Tiller, Phys. Status Solidi **130**, 131 (1985).

[35]T. Takai, T. Halicioğlu, and W. A. Tiller, Phys. Status Solidi **130**, 475 (1985).

[36]J. E. Jones, Proc. R. Soc. London, Ser. A **106**, 463 (1924).

[37]B. M. Axilrod and E. Teller, J. Chem. Phys. **11**, 299 (1943).

[38]P. N. Keating, Phys. Rev. **145**, 637 (1966).

[39]R. Biswas and D. R. Hamann, Phys. Rev. B **36**, 6434 (1987).

[40]R. Biswas and D. R. Hamann, Phys. Rev. Lett. **55**, 2001 (1985).

[41]J. Tersoff, Phys. Rev. Lett. **56**, 632 (1986).

[42]J. Tersoff, Phys. Rev. B **37**, 6991 (1988).

[43]F. H. Stillinger, and T. A. Weber, Phys. Rev. B **31**, 5262 (1985).

[44]I. NoorBatcha, L. M. Raff, and D. L. Thompson, J. Chem. Phys. **81**, 3715 (1984).

[45]D. W. Brenner and B. J. Garrison, Phys. Rev. B **34**, 1304 (1986).

[46]J. Lampinen, R. M. Nieminen, and K. Kaski, Surf. Sci. **200**, 101 (1988).

[47]A. Schneider, I. K. Schuller, and A. Rahman, Phys. Rev. B **36**, 1340 (1987).

[48]W. D. Leudtke and U. Landman, Phys. Rev. B **37**, 4656 (1988).

[49]U. Landman, W. D. Luedtke, R. N. Barnett, C. L. Cleveland, M. W. Ribarsky, E. Arnold, S. Ramesh, H. Baumgart, A. Martinez, and B. Khan, Phys. Rev. Lett. **56**, 155 (1986).

[50]M. D. Kluge, J. R. Ray, and A. Rahman, J. Chem. Phys. **87**, 2336 (1987).

[51]U. Landman, W. D. Luedtke, M. W. Ribarsky, R. N. Barnett, and C. L. Cleveland, Phys. Rev. B **37**, 4637 (1988).

[52]W. D. Luedtke, U. Landman, M. W. Ribarsky, R. N. Barnett, and C. L. Cleveland, Phys. Rev. B **37**, 4647 (1988).

[53]B. P. Feuston, R. K. Kalia, and P. Vashishta, Phys. Rev. B **35**, 6222 (1987).

[54]M. D. Kluge, J. R. Ray, and A. Rahman, J. Chem. Phys. **85**, 4028 (1986).

[55]D. E. Harrison, Jr., W. L. Moore, Jr., and H. T. Holcombe, Rad. Eff. **17**, 167 (1973).

[56]D. E. Harrison, Jr. and D. S. Greiling, J. Appl. Phys. **38**, 3200 (1967).
[57]R. E. Schlier and H. E. Farnsworth, J. Chem. Phys. **30**, 917 (1959).
[58]J. J. Lander and J. Morrison, J. Chem. Phys. **37**, 729 (1962).
[59]D. J. Chadi, Phys. Rev. Lett. **43**, 43 (1979).
[60]M. T. Yin and M. L. Cohen, Phys. Rev. B **24**, 2303 (1981).
[61]M. Schlüter, in *Surface Properties of Electronic Materials (The Chemical Physics of Solid Surfaces and Heterogeneous Catalysis)*, edited by D. A. King and D. P. Woodruff (Elsevier, Amsterdam, 1988), Vol. 5, Chap. 2.
[62]M. T. Robinson, in *Sputtering by Particle Bombardment I (Topics in Applied Physics 47)*, edited by R. Behrisch (Springer-Verlag, Heidelberg, 1981), Chap. 3.
[63]F. F. Abraham and I. P. Batra, Surf. Sci. **163**, L752 (1985).
[64]F. Bechstedt and D. Reichardt, Surf. Sci. **202**, 83 (1988).
[65]R. M. Tromp, R. J. Hamers, and J. E. Demuth, Phys. Rev. Lett. **55**, 1303 (1985).
[66]R. J. Hamers, R. M. Tromp, and J. E. Demuth, Phys. Rev. B **34**, 5347 (1986).
[67]E. T. Gawlinski and J. D. Gunton, Phys. Rev. B **36**, 4774 (1987).
[68]J. Lampinen, R. M. Nieminen, and K. Kaski, Surf. Sci. **203**, 201 (1988).
[69]F. F. Abraham and J. Q. Broughton, Phys. Rev. Lett. **56**, 734 (1986).
[70]X.-P. Li, P. B. Allen, and J. Q. Broughton, Phys. Rev. Lett. **61**, 243 (1988).
[71]D. W. Brenner and B. J. Garrison, Surf. Sci. **198**, 151 (1988).
[72]P. M. Agrawal, L. M. Raff, and D. L. Thompson, Surf. Sci. **188**, 402 (1987).
[73]B. J. Garrison, M. T. Miller, and D. W. Brenner, Chem. Phys. Lett. **146**, 553 (1988).
[74]D. Ostry and R. J. MacDonald, Phys. Lett. A **32**, 303 (1970).
[75]R. J. MacDonald, D. Ostry, E. Zwangobani, and E. Dennis, Ned. Tijdschr. Vacuümtech. **8**, 207 (1970).
[76]G. L. Smith, M. Sc. thesis, Naval Postgraduate School, 1977.
[77]D. E. Harrison, Jr., N. S. Levy, J. P. Johnson III, and H. M. Effron, J. Appl. Phys. **39**, 3742 (1968).
[78]A. A. Abrahamson, Phys. Rev. **178**, 76 (1969).
[79]P. T. Wedepohl, Proc. Phys. Soc. **92**, 79 (1967).
[80]D. E. Harrison, Jr., Bull. Am. Phys. Soc. II **14**, 315 (1969).
[81]W. D. Wilson and C. L. Bisson, Phys. Rev. B **3**, 3984 (1971).
[82]S. C. Park and D. C. Clary, J. Appl. Phys. **60**, 1183 (1986).
[83]P. Blank and K. Wittmaack, J. Appl. Phys. **50**, 1519 (1979).
[84]J. Kempf, Appl. Phys. **16**, 43 (1978).
[85]R. J. MacDonald, Rad. Eff. **3**, 131 (1970).
[86]R. J. MacDonald, Philos. Mag. **21**, 519 (1970).
[87]H. H. Andersen and H. L. Bay, in *Sputtering by Particle Bombardment I (Topics in Applied Physics 47)*, edited by R. Behrisch (Springer-Verlag, Heidelberg, 1981), Chap. 4.
[88]N. Winograd, P. H. Kobrin, G. A. Schick, J. Singh, J. P. Baxter, and B. J. Garrison, Surf. Sci. **176**, L817 (1986).
[89]K. Broomfield, R. A. Stansfield, and D. C. Clary, Surf. Sci. **202**, 320 (1988).
[90]D. R. J. Boyd, J. Chem. Phys. **23**, 922 (1955).
[91]S. Rothenberg, R. H. Young, and H. F. Schaefer III, J. Am. Chem. Soc. **92**, 3243 (1970).
[92]A. Veillard, Theo. Chim. Acta **12**, 405 (1968).
[93]*Gaussian Basis Sets for Molecular Calculations, Physical Sciences Data 16,* edited by S. Huzinaga, J. Andzelm, M. Klobukowski, E. Radzio-Andzelm, Y. Sakai, and H. Tatewaki (Elsevier, Amsterdam, 1984).
[94]T. H. Dunning, Jr., J. Chem. Phys. **53**, 2823 (1970).
[95]T. H. Dunning, Jr. and P. J. Hay, in *Methods of Electronic Structure Theory (Modern Theoretical Chemistry),* edited by H. F. Schaefer III (Plenum, New York, 1977), Vol. 3, Chap. 1.
[96]R. D. Amos, The Cambridge Analytic Derivatives Package (CADPAC), Science and Engineering Research Council report no. CCP1/84/4 (Daresbury Laboratory, 1984, unpublished).
[97]P. Saxe, D. J. Fox, H. F. Schaefer III, and N. C. Handy, J. Chem. Phys. **77**, 5584 (1982).
[98]Numerical Analysis Group (NAG) subroutine library Mark 11, Numerical Analysis Group, Oxford, 1984.
[99]*Handbook of Mathematical Functions,* edited by M. Abramowitz and I. A. Stegun (Dover, New York, 1965), Chap. 22.
[100]J. P. Biersack and J. F. Ziegler, Nucl. Instrum. Methods **194**, 93 (1982).
[101]G. Molière, Z. Naturforsch. **2a**, 133 (1947).
[102]D. J. O'Connor and J. P. Biersack, Nucl. Instrum. Methods B **15**, 14 (1986).
[103]D. G. Truhlar and J. T. Muckerman, in *Atom-Molecule Collision Theory: A Guide for the Experimentalist,* edited by R. B. Bernstein (Plenum, New York, 1979), Chap. 16.
[104]D. E. Harrison, Jr., J. Appl. Phys. **52**, 1499 (1981).
[105]D. E. Harrison, Jr., Rad. Eff. **70**, 1 (1983).
[106]A. L. Southern, W. R. Willis, and M. T. Robinson, J. Appl. Phys. **34**, 153 (1963).
[107]J. W. Coburn, H. F. Winters, and T. J. Chuang, J. Appl. Phys. **48**, 3532 (1977).
[108]S. Tachi, K. Miyake, and T. Tokuyama, Jpn. J. Appl. Phys. **21** (Suppl. 21-1), 141 (1982).
[109]S. T. Kang, R. Shimizu, and T. Okutani, Jpn. J. Appl. Phys. **18**, 1717 (1979).
[110]P. C. Zalm, J. Appl. Phys. **54**, 2660 (1983).
[111]N. Laegreid and G. K. Wehner, J. Appl. Phys. **32**, 365 (1961).
[112]D. Rosenberg and G. K. Wehner, J. Appl. Phys. **33**, 1842 (1962).
[113]S. Tachi and S. Okudaira, J. Vac. Sci. Technol. B **4**, 459 (1986).
[114]J. M. F. Harper, J. J. Cuomo, P. A. Leary, G. M. Summa, H. R. Kaufmann, and F. J. Bresnock, J. Electrochem. Soc. **128**, 1077 (1981).
[115]J. Kirschner and H. W. Etzkom, Appl. Surf. Sci. **3**, 351 (1979).
[116]P. Blank and K. Wittmaack, Phys. Lett. **54A**, 33 (1975).
[117]Y. Okajima, J. Appl. Phys. **51**, 715 (1980).
[118]P. C. Zalm, L. J. Beckers, and F. H. M. Sanders, Nucl. Instrum. Methods **209/210**, 561 (1983).
[119]J. W. Mayer, L. Eriksson, and J. A. Davies, *Ion Implantation in Semiconductors* (Academic, New York, 1970), pp. 76–97.
[120]P. Sigmund, Phys. Rev. **184**, 383 (1969).
[121]D. E. Harrison, Jr. and R. P. Webb, J. Appl. Phys. **53**, 4193 (1982).
[122]D. E. Harrison, Jr., J. Appl. Phys. **52**, 4251 (1981).
[123]M. H. Shapiro, P. K. Haff, T. A. Tombrello, D. E. Harrison, Jr., and R. P. Webb, Rad. Eff. **89**, 234 (1985).
[124]D. E. Harrison, Jr., J. Appl. Phys. **52**, 1499 (1981).
[125]M. W. Thompson, Philos. Mag. **18**, 377 (1968).
[126]M. W. Thompson, Phys. Rep. **69**, 336 (1981).
[127]B. J. Garrison, Nucl. Instrum. Methods B **17**, 305 (1986).
[128]R. A. Gibbs, S. P. Holland, K. E. Foley, B. J. Garrison, and N. Winograd, J. Chem. Phys. **76**, 684 (1982).
[129]B. J. Garrison, N. Winograd, D. M. Deaven, C. T. Reimann, D. Y. Lo, T. A. Tombrello, D. E. Harrison, Jr., and M. H. Shapiro, Phys. Rev. B **37**, 7197 (1988).

[130]B. W. Farmery and M. W. Thompson, Philos. Mag. **18**, 415 (1968).
[131]A. R. Bayly and R. J. MacDonald, Rad. Eff. **34**, 169 (1977).
[132]B. J. Garrison, N. Winograd, and D. E. Harrison, Jr., Surf. Sci. **87**, 101 (1979).
[133]B. J. Garrison, C. T. Reimann, N. Winograd, and D. E. Harrison, Jr., Phys. Rev. B **36**, 3516 (1987).
[134]T. Okutani, M. Shikata, S. Ichimura, and R. Shimizu, J. Appl. Phys. **51**, 2884 (1980).
[135]B. Emmoth and M. Braun, Phys. Scr. **24**, 415 (1981).
[136]H. Tsuge and S. Esho, J. Appl. Phys. **52**, 4391 (1981).
[137]R. S. Nelson and D. J. Mazey, Can. J. Phys. **46**, 689 (1968).
[138]G. S. Anderson, J. Appl. Phys. **37**, 3455 (1966).
[139]G. S. Anderson, J. Appl. Phys. **38**, 1607 (1967).
[140]N. Winograd, B. J. Garrison, and D. E. Harrison, Jr., Phys. Rev. Lett. **41**, 1120 (1978).
[141]R. E. Hönig, J. Appl. Phys. **29**, 549 (1958).
[142]K. Wittmaack, Phys. Lett. A **69**, 322 (1979).
[143]C.-E. Richter and M. Trapp, Int. J. Mass. Spectrom. Ion Phys. **38**, 21 (1981).
[144]T. T. Tsong, J. Vac. Sci. Technol. B **3**, 1425 (1985).
[145]J. R. Woodyard and C. B. Cooper, J. Appl. Phys. **35**, 1107 (1964).
[146]G. Staudenmaier, Rad. Eff. **13**, 87 (1972).
[147]B. J. Garrison and N. Winograd, Science **216**, 805 (1982).
[148]R. G. Orth, H. T. Jonkman, D. H. Powell, and J. Michl, J. Am. Chem. Soc. **103**, 6026 (1981).
[149]K. E. Foley, N. Winograd, B. J. Garrison, and D. E. Harrison, Jr., J. Chem. Phys. **80**, 5254 (1984).
[150]D. E. Harrison, Jr. and C. B. Delaplain, J. Appl. Phys. **47**, 2252 (1976).
[151]B. J. Garrison, N. Winograd, and D. E. Harrison, Jr., J. Chem. Phys. **69**, 1440 (1978).
[152]N. Winograd, D. E. Harrison, Jr., and B. J. Garrison, Surf. Sci. **78**, 467 (1978).
[153]N. Winograd, K. E. Foley, B. J. Garrison, and D. E. Harrison, Jr., Phys. Lett. **73A**, 253 (1979).
[154]B. J. Garrison and N. Winograd, Chem. Phys. Lett. **97**, 381 (1983).
[155]N. Winograd, B. J. Garrison, T. Fleisch, W. N. Delgass, and D. E. Harrison, Jr., J. Vac. Sci. Technol. **16**, 629 (1979).
[156]D. E. Harrison, Jr., Ph. Avouris, and R. Walkup, Nucl. Instrum. Methods B **18**, 349 (1987).
[157]B. J. Garrison, N. Winograd, and D. E. Harrison, Jr., J. Vac. Sci. Technol. **16**, 789 (1979).
[158]A. Benninghoven, Surf. Sci. **53**, 596 (1975).
[159]A. Benninghoven, K. H. Muller, C. Plog, M. Schummer, and P. Steffens, Surf. Sci. **63**, 403 (1977).
[160]P. Joyes, J. Phys. B **4**, L15 (1971).
[161]K. Wittmaack, Phys. Lett. A **69**, 322 (1979).
[162]L. A. Girifalco and V. G. Weizer, Phys. Rev. **114**, 687 (1959).